

# CoFOLD: thermodynamic RNA structure prediction with a kinetic twist

Jeff R. Proctor and Irmtraud M. Meyer

Centre for High-Throughput Biology & Department of Computer Science and  
Department of Medical Genetics, University of British Columbia,  
2125 East Mall, Vancouver, BC,  
Canada V6T 1Z4, irmtraud.meyer@cantab.net

July 15, 2012

**Running head:** co-transcriptional RNA folding, RNA structure prediction, RNA secondary structures

**Summary:** Existing state-of-the-art methods that take a single RNA sequence and predict the corresponding RNA  $\beta$  are thermodynamic methods. These predict the most stable RNA structure, but do not consider the process of structure formation. We have by now ample experimental and theoretical evidence, however, that sequences *in vivo* fold while being transcribed and that the process of structure formation matters. We here present a conceptually new method for predicting RNA  $\beta$ , called CoFOLD, that combines thermodynamic with kinetic considerations. Our method significantly improves the state-of-art in terms of prediction accuracy, especially for long sequences of more than a thousand nucleotides length such as ribosomal RNAs.

**Introduction:** The primary products of almost all genomes are transcripts, *i.e.* RNA sequences. Their expression is often regulated by RNA structure which forms when the transcript interacts with itself via hydrogen-bonds between complementary nucleotides (G-C, A-U, G-U). These structures regulate translation, transcription, splicing, RNA editing and transcript degradation. To assign a potential functional role to a transcript, it often suffices to know its RNA  $\beta$ , *i.e.* the set of base pairs. As entire transcriptomes are now routinely sequenced, computational methods that predict RNA  $\beta$  for individual input RNA sequences play a key role in annotating new transcripts. This is emphasised by the fact that the majority of mammalian genomes is transcribed into transcripts of unknown function<sup>1,2</sup> and that experimental techniques for RNA structure determination such as X-ray crystallography and NMR remain costly and slow.

More than three decades of research have been invested into devising methods that take a single RNA sequence and predict its RNA  $\beta$ . When homologous sequences from related species are scarce or not available, non-comparative methods such as RNAFOLD<sup>3</sup> and MFOLD<sup>4</sup> provide the state-of-art in terms of prediction accuracy. They employ an optimisation strategy that searches the space of potential  $\beta$ s for the most stable structure and depend on hundreds of free

energy parameters that have been initially experimentally determined<sup>5</sup> and computationally tweaked<sup>6</sup>. Recent attempts at replacing these thermodynamic parameters by probabilistic ones have led to a similar or slightly improved prediction accuracy<sup>7</sup>. All non-comparative thermodynamic methods, however, show a marked drop in performance accuracy for increased sequence lengths.

Key experiments<sup>8,9,10</sup> from the early 1980s show that structure formation happens co-transcriptionally, *i.e.* while the RNA is being transcribed. Many experiments<sup>11,12,13,14,15,16,17,18,19</sup> have since substantiated this view. In 1996, Morgan and Higgs<sup>20</sup> studied the discrepancies between the conserved RNA  $\beta$ s and the corresponding, predicted minimum free energy (MFE) structures for long RNA sequences and concluded that these differences “cannot simply be put down to errors in the free energy parameters used in the model”. They hypothesised that these differences may be due to effects of kinetic folding. These results are complemented by statistical evidence that structured transcripts not only encode information on the functional RNA structure, but also on their co-transcriptional folding pathway<sup>21</sup>. While there is thus ample evidence that the process of structure formation matters to the formation of the functional structure *in vivo*, it is ignored by thermodynamic methods for RNA  $\beta$  prediction.

Several sophisticated computational methods have already been devised that explicitly mimic the co-transcriptional structure formation *in vivo*<sup>22,23,24,25,26,27,28,29,30</sup>. These folding pathway prediction methods make a range of simplifying assumptions and approximations of the complex *in vivo* environment. So far, these methods have only been used to study a few select and typically short ( $\ll$  1000 nt) sequences and an evaluation of their prediction accuracy is currently missing.

We here propose a conceptually new method, called CoFOLD, that combines the benefits of a deterministic, thermodynamic method with kinetic considerations that capture effects of the structure formation process. For this, we build upon the state-of-the-art method RNAFOLD<sup>3</sup> by combining its thermodynamic energy scores with a scaling function. We train the two free parameters of CoFOLD on a large and diverse data set of 248 sequences and examine the predictive power of CoFOLD on a non-redundant data set of 61 long sequences ( $>$  1000 nt). CoFOLD shows a significant improvement in prediction accuracy, in particular for long RNA sequences such as ribosomal RNAs.

	TPR (%)	FPR (%)	PPV (%)	MCC (%)
RNAFOLD	46.30	0.0176	39.74	42.81
RNAFOLD-A	52.02	0.0160	44.76	48.17
CoFOLD	52.83	0.0159	45.79	49.10
CoFOLD-A	57.80	0.0145	50.06	53.70

**Table 1. Prediction accuracy of CoFOLD for base pairs.** The performance accuracy of CoFOLD, CoFOLD-A, RNAFOLD and RNAFOLD-A for the long data set in terms of true positive rate ( $TPR = 100 \cdot TP / (TP + FN)$ ), false positive rate ( $FPR = 100 \cdot FP / (FP + TN)$ ), positive predictive value ( $PPV = 100 \cdot TP / (TP + FP)$ ) and Matthew’s correlation coefficient ( $MCC = 100 \cdot (TP \cdot TN - FP \cdot FN) / \sqrt{(TP + FP) \cdot (TP + FN) \cdot (TN + FP) \cdot (TN + FN)}$ ), where TP denotes the numbers of true positives, TN the true negatives, FP the false positives and FN the false negatives.

**Folding long RNA sequences** We evaluate the prediction accuracy of CoFOLD by comparing the  $\beta$  predicted by CoFOLD to the known reference  $\beta$ s for a test set of 61 long sequences (long data set). We compile this data set by identifying sequences that are long ( $> 1000$  nt), correspond to biological sequences, have reference structures that are supported by phylogenetic evidence and are non-redundant in terms of pairwise percent sequence identify (max 85%) and evolutionary distance (Supplementary Information, Section 1, Table 2, Table 3 and Table 4). These selection criteria yield a data set of 16S ribosomal RNA (rRNA) and 23S rRNA sequences from archaea, bacteria, eukaryotes and chloroplasts with an average length of 2397 nt (min 1245 nt, max 3578 nt).

Compared to RNAFOLD which is the state-of-the-art thermodynamic RNA structure prediction method, CoFOLD predicts 7% more known base pairs at 6% higher specificity than RNAFOLD thereby increasing the Matthew’s correlation coefficient (MCC) by 6% (MCC (RNAFOLD) = 42.81%, MCC (CoFOLD) = 49.10%) (Table 1, Supplementary Information, Section 2). This improvement in overall performance accuracy can be attributed to a simultaneous increase of the positive predictive value (PPV) and the true positive rate (TPR) for almost all individual sequences (Figure 1) and a simultaneous slight decrease of the false positive rate (FPR) (Supplementary Information, Section 2 and Figure 5). Both RNAFOLD and CoFOLD employ the default Turner 1999 free energy parameters<sup>5</sup>. Combining CoFOLD with the Andronescu 2007 free energy parameters<sup>6</sup> (CoFOLD-A) increases the sensitivity and specificity by a further 4% (MCC (CoFOLD-A) = 53.70%). Doing the same with RNAFOLD (RNAFOLD-A) also increases the sensitivity and specificity with respect to RNAFOLD, but results in a smaller performance increase than for CoFOLD (MCC (RNAFOLD-A) = 48.17%, MCC (CoFOLD) = 49.10%). Whereas CoFOLD only depends on two free parameters, the Andronescu 2007 free energy model<sup>6</sup> comprises 363 free parameters that were trained using machine learning techniques (Supplementary Information, Section 3).

**Explicitly capturing the structure formation process** In order to capture effects of co-transcriptional folding in CoFOLD, we introduce a scaling function  $\gamma(d)$ . This function scales the nominal energy contribution of any base-pair-like interaction depending on the distance  $d$  of the interaction partners along the sequence (Supplementary Information, Section 3 and

Figure 6). It thereby captures that during the structure formation process, potential pairing partners in close proximity are easier to identify than more distant ones. This scaling amounts to a re-weighting of the structure search space that the structure prediction algorithm explores. Rather than guiding the structure prediction solely based on thermodynamic considerations as the state-of-the-art methods RNAFOLD and MFOLD<sup>4</sup> do, CoFOLD thus combines kinetic and thermodynamic considerations.

The scaling function of CoFOLD depends on two free parameters,  $\alpha$  and  $\tau$  which have a straightforward interpretation (Supplementary Information, Section 3 and Figure 6). Our goal in training the two parameters was to confirm that parameter training is robust and to ensure that CoFOLD can be applied across a wide range of sequence lengths.

To this end, we compiled an extended data set of 248 sequences (combined data set) which comprises the 61 long sequences of the long data set and, in addition, 187 short sequences ( $\leq 1000$  nt length) that also correspond to biological sequences whose reference structures are supported by phylogenetic evidence (Supplementary Information, Section 1, Table 2, Table 3 and Table 4). The sequences in this combined data set have an average length of 776 nt (min 110 nt, max 3578 nt). Using twenty trials of five-fold cross-validation for parameter training, we find that the optimal prediction accuracy in terms of average MCC is obtained by a combination of  $\alpha$  and  $\tau$  values whose strong correlation can be described by a linear function  $\alpha = a \cdot \tau + b$ , where  $a = 6.1 \cdot 10^{-4} \pm 2 \cdot 10^{-5}$  is the slope and  $b = 0.105 \pm 0.016$  the intercept ( $R^2 = 98.4\%$ ) (Supplementary Information, Section 4 and Figure 8 (left)). Our cross-evaluation experiments yield optimal parameter combinations that fall within or near the 95% confidence interval around the linear fit, thus confirming the robustness of parameter training (Supplementary Information, Figure 8 (right)). We use  $\alpha = 0.50$  and  $\tau = 640$  in CoFOLD and CoFOLD-A (Supplementary Information, Figure 6).

CoFOLD and CoFOLD-A outperform RNAFOLD and RNAFOLD-A also for short sequences ( $\leq 1000$  nt), although the improvement in terms of MCC is less pronounced than for long sequences (Supplementary Information, Table 5). RNAFOLD shows a slight decrease in prediction accuracy when used with the Andronescu 2007 parameters. The behaviour of CoFOLD is in line with our expectation that the beneficial impact of modelling co-transcriptional folding decreases for short sequences.

We conclude that CoFOLD effectively depends only on one free parameter and that CoFOLD and CoFOLD-A increase the prediction accuracy for all sequence lengths, in particular for long sequences ( $> 1000$  nt).

### **Capturing structure formation yields improved structures of similar free energies**

In order to examine if capturing the effects of co-transcriptional folding significantly changes the free energies of the predicted structures, we calculated the free energies of the structures predicted by CoFOLD, CoFOLD-A and RNAFOLD-A and compared them to the free energies of the corresponding structures predicted by RNAFOLD. To ensure consistency, we used the Turner 1999 energy parameters to calculate the energies of all predicted RNA structures.

The structures predicted by CoFOLD for the long data set differ on average by 2% from the respective free energies of the corresponding structures predicted by RNAFOLD and the distribution of relative energy differences is comparatively tight (stdev = 1.0%, min = 0.2%, max = 4.4%) (Figure 2 and Supplementary Information, Table 6). Combining CoFOLD and RNAFOLD with

the Andronescu 2007 energy parameters significantly increases the average free energy difference (5% (RNAFOLD-A), 7% (CoFOLD-A)), broadens the distributions ( $\text{stdev}(\text{RNAFOLD-A}) = 1.9\%$ ,  $\text{stdev}(\text{CoFOLD-A}) = 2.4\%$ ) and leads to higher maximum energy differences ( $\text{max}(\text{RNAFOLD-A}) = 11.1\%$ ,  $\text{max}(\text{CoFOLD-A}) = 13.1\%$ ). For short sequences, these differences are even more pronounced (Supplementary Information, Table 6).

Most importantly, a large energy difference with respect to the free energy of the structure predicted by RNAFOLD does not imply an increased prediction accuracy, neither for short nor long sequences and for none of the prediction programs (Supplementary Information, Figure 11 and Table 7).

To summarise, CoFOLD significantly increases the prediction accuracy without significantly altering the free energies of the structures that RNAFOLD would predict for the same input sequences.

**Folding ribosomal RNAs** 23S ribosomal RNAs are the longest sequences of the long data set with an average length of 3069 nt (min 2882 nt, max 3578 nt) and are thus some of the most challenging RNA structures to predict. Using CoFOLD and CoFOLD-A, we increase their prediction accuracy in terms of MCC w.r.t. RNAFOLD on average by 8% and 12%, respectively. Figure 3 shows, for the 23S rRNA of the gamma-proteobacteria *Pseudomonas aeruginosa*, how the RNA structure predicted by CoFOLD-A compares to that predicted by RNAFOLD. The most apparent differences are that RNAFOLD predicts many incorrect mid- and long-range base pairs (red arcs spanning more than 100 nt) and that almost all of these disappear with CoFOLD-A. In addition, CoFOLD-A adds many correct mid- and long-range base pairs (blue arcs), see in particular those spanning almost the entire sequence. Overall, CoFOLD-A increases the MCC of RNAFOLD from 43% to 58%. This 15% rise in performance accuracy is due to a significant increase of the true positive rate (45%  $\rightarrow$  61%) and an equally significant increase of the positive predictive value (41%  $\rightarrow$  56%). This is in-line with is the typical behaviour seen for CoFOLD (Figure 1 and Supplementary Information, Figure 5). The false positive rate for both prediction methods remains low at 0.01%.

We also investigated the performance for the 16S ribosomal RNAs in greater detail. With an average length of 1550 nt (min 1245 nt, max 1799 nt), these are significantly shorter than the 23S rRNAs in our long data set, but still considerably longer than the average test sequence on which thermodynamic prediction methods are typically benchmarked. Figure 4 shows the improvements in prediction accuracy for the 16S rRNA of the freshwater algae *Cryptomonas sp.* (species unknown). This ribosomal sequence is 1493 nt long. CoFOLD-A improves the prediction accuracy of RNAFOLD from an MCC of 32% to 73%. This 41% improvement in performance accuracy is achieved by significantly reducing the number of erroneously predicted mid- to long-range base pairs (red arcs spanning more than 100 nt) while simultaneously increasing the number of correctly predicted base pairs in wide distance range (blue arcs). This is reflected by the simultaneous increase of the true positive rate (33%  $\rightarrow$  77%) and the positive predictive value (30%  $\rightarrow$  69%) which, in this example, is also accompanied by a slight reduction of the false positive rate (0.03%  $\rightarrow$  0.01%).

As neither CoFOLD nor RNAFOLD are technically capable of predicting pseudo-knotted features, the pseudo-knotted reference structures of the 23S rRNA and the 16S rRNA cannot be predicted with perfect accuracy (see orange arcs in Figure 3 and Figure 4).

**Discussion** Our results show that the state-of-the-art in non-comparative RNA  $\beta$  prediction can be significantly improved by capturing effects of the structure formation process. To this end, we introduce a conceptually new RNA  $\beta$  prediction method called CoFOLD which judges the reachability of potential pairing partners during co-transcriptional structure formation via a scaling function. We reliably train the two free parameters of CoFOLD using a large and diverse data set of 248 sequences. This scaling function effectively depends on only one free parameter which has a straightforward interpretation as it determines how the reachability declines as function of the nucleotide distance. Without altering the free energy parameters of the underlying thermodynamic model, CoFOLD thereby guides the structure prediction process by a combination of thermodynamic and kinetic considerations. It thereby arrives at significantly more accurate structure predictions, in particular for long sequences ( $> 1000$  nt) such as ribosomal RNAs. The significance of the improvement in prediction accuracy is underlined by the improvement in sensitivity and specificity for the individual sequences. Most importantly, this improvement is gained without significantly shifting the free energies of the predicted RNA structures. We thereby confirm Morgan and Higgs<sup>20</sup> who hypothesised that discrepancies between the functional RNA  $\beta$  and the corresponding minimum free energy structures predicted by thermodynamic methods such as RNAfold are not due to errors of the underlying free energy parameters, but due to a lack of modelling the effects of kinetic structure formation.

Many sophisticated experiments<sup>8,9,10,11,12,13,14,15,16,17,18,19</sup> paint a dauntingly complex picture of co-transcriptional structure formation *in vivo* which can depend on a multitude of factors ranging from the speed of transcription and the variation thereof, to a range of carefully orchestrated *cis* and *trans* interactions with a variety of other molecules.

Several sophisticated folding pathway prediction methods have already been devised that explicitly mimic the co-transcriptional structure formation *in vivo*<sup>22,23,24,25,26,27,28,29,30</sup>. Even though these methods need to make a range of simplifying assumptions to approximate the complex *in vivo* environment and have so far been only used to investigate a few select and typically short ( $\ll 1000$  nt) sequences, these methods have already allowed us to gain valuable and detailed insight into co-transcriptional folding pathways<sup>26,31</sup>.

By proposing a conceptually new approach to RNA  $\beta$  prediction, CoFOLD, we show that it is possible to capture effects of the structure formation process in deterministic thermodynamic methods and that the benefits of doing so are significant, both in terms of prediction accuracy and insight gained. This finding is not too surprising given that any co-transcriptionally emerging RNA transcript *in vivo* needs to find a way to actually reach the functionally relevant RNA structure. Although CoFOLD only constitutes the first attempt at explicitly capturing the effects of co-transcriptional folding in a thermodynamic RNA  $\beta$  prediction program, we hope that our results will inspire a new generation of these methods that explicitly capture aspects of the structure formation process *in vivo*. Recent developments in experimental techniques<sup>17,19</sup> will no doubt significantly contribute to our understanding of structure formation *in vivo*. We are thus looking forward to joint projects between the experimental and theoretical RNA structure community.

**Methods summary** The algorithm of CoFOLD and the scoring function are described in detail in the Supplementary Information. CoFOLD is publicly available on the Internet via a web-server at <http://www.e-rna.org/cofold>.

## References

1. Mattick, J. S. & Makunin, I. V. Non-coding RNA. *Hum Mol Gen* **15**, R17–R29 (2006).
2. Carninci, P. *et al.* The transcriptional landscape of the mammalian genome. *Science* **309**, 1559–1563 (2005).
3. Zuker, M. & Stiegler, P. Optimal computer folding of large RNA sequences using thermodynamic and auxiliary information. *Nucleic Acids Res* **9**, 133–148 (1981).
4. Zuker, M. Mfold web server for nucleic acid folding and hybridization prediction. *Nucleic Acids Res* **31**, 3406–3415 (2003).
5. Mathews, D. H., Sabina, J., Zuker, M. & Turner, D. H. Expanded sequence dependence of thermodynamic parameters improves prediction of RNA secondary structure. *J Mol Biol* **288**, 911–940 (1999).
6. Andronescu, M., Condon, A., Hoos, H. H., Mathews, D. H. & Murphy, K. P. Efficient parameter estimation for RNA secondary structure prediction. *Bioinformatics* **23**, I19–I28 (2007).
7. Rivas, E., Lang, R. & Eddy, S. E. A range of complex probabilistic models for RNA secondary structure prediction that includes the nearest-neighbor model and more. *RNA* **18**, 193–212 (2012).
8. Boyle, J., Robillard, G. & Kim, S. Sequential folding of transfer RNA. A nuclear magnetic resonance study of successively longer tRNA fragments with a common 5' end. *J Mol Biol* **139**, 601–625 (1980).
9. Kramer, F. & Mills, D. Secondary structure formation during RNA-synthesis. *Nucleic Acids Res* **9**, 5109–5124 (1981).
10. Brehm, S. & Cech, T. Fate of an intervening sequence ribonucleic-acid — excision and cyclization of the Tetrahymena ribosomal ribonucleic-acid intervening sequence *in vivo*. *Biochemistry* **22**, 2390–2397 (1983).
11. Lewicki, B., Margus, T., Remme, J. & Nierhaus, K. Coupling of rRNA transcription and ribosomal assembly *in vivo* – formation of active ribosomal-subunits in *Escherichia coli* requires transcription of RNA genes by host RNA polymerase which cannot be replaced by T7 RNA polymerase. *J Mol Biol* **231**, 581–593 (1993).
12. Chao, M. Y., Kan, M. & Lin-Chao, S. RNAII transcribed by IPTG-induced T7 RNA polymerase is non-functional as a replication primer for ColE1-type plasmids in *Escherichia coli*. *Nucleic Acids Res* **23**, 1691–1695 (1995).
13. Pan, T., Fang, X. & Sosnick, T. Pathway modulation, circular permutation and rapid RNA folding under kinetic control. *J Mol Biol* **286**, 721–731 (1999).

14. Heilman-Miller, S. & Woodson, S. Effect of transcription on folding of the Tetrahymena ribozyme. *RNA* **9**, 722–733 (2003).
15. Heilman-Miller, S. & Woodson, S. Perturbed folding kinetics of circularly permuted RNAs with altered topology. *J Mol Biol* **328**, 385–394 (2003).
16. Mahen, E., Harger, J., Calderon, E. & Fedor, M. Kinetics and thermodynamics make different contributions to RNA folding in vitro and in yeast. *Mol Cell* **19**, 27–37 (2005).
17. Adilakshmi, T., Soper, S. & Woodson, S. Structural analysis of RNA in living cells by in vivo synchrotron x-ray footprinting. *Methods Enzymol* **468**, 239–259 (2009).
18. Mahen, E., Watson, P., Cottrell, J. & Fedor, M. mRNA Secondary Structures Fold Sequentially But Exchange Rapidly In Vivo. *PLoS Biol* **8**, e1000307 (2010).
19. Woodson, S. A. Compact Intermediates in RNA folding. *Annual Review of Biophysics* **39**, 61–77 (2010).
20. Morgan, S. & Higgs, P. Evidence for kinetic effects in the folding of large RNA molecules. *J Chem Phys* **105**, 7152–7157 (1996).
21. Meyer, I. M. & Miklós, I. Co-transcriptional folding is encoded within RNA genes. *BMC Mol Biol* **10**, 5 (2004).
22. Mironov, A., Dyakonova, L. & Kister, A. A kinetic approach to the prediction of RNA secondary structures. *J Biomol Struct Dyn* **2**, 953–962 (1985).
23. Mironov, A. & Lebedev, V. A kinetic model of RNA folding. *Biosystems* **30**, 49–56 (1993).
24. Gulyaev, A., von Batenburg, F. & Pleij, C. The computer-simulation of RNA folding pathways using a genetic algorithm. *J Mol Biol* **250**, 37–51 (1995).
25. Flamm, C., Fontana, W., Hofacker, I. L. & Schuster, P. RNA folding at elementary step resolution. *RNA* **6**, 325–338 (2000).
26. Isambert, H. & Siggia, E. D. Modeling RNA folding paths with pseudoknots: application to hepatitis delta virus ribozyme. *PNAS* **97**, 6515–6520 (2000).
27. Xayaphoummine, A., Bucher, T., Thalmann, F. & Isambert, H. Prediction and statistics of pseudoknots in RNA structures using exactly clustered stochastic simulations. *PNAS* **100**, 15310–15315 (2003).
28. Xayaphoummine, A., Bucher, T. & Isambert, H. Kinefold web server for RNA/DNA folding path and structure prediction including pseudoknots and knots. *Nucleic Acids Res* **33**, W605–610 (2005).
29. Danilova, L., Pervouchine, D., Favorov, A. & Mironov, A. RNAkinetics: a web server that models secondary structure kinetics of an elongating RNA. *Journal of Bioinformatics and Computational Biology* **4**, 589–596 (2006).



30. Geis, M. *et al.* Folding kinetics of large RNAs. *J Mol Biol* **379**, 160–173 (2008).
31. Schoemaker, R. J. W. & Gulyaev, A. P. Computer simulation of chaperone effects of Archaeal C/D box sRNA binding on rRNA folding. *Nucleic Acids Res* **34**, 2015–2026 (2006).
32. Lai, D., Proctor, J. R., Zhu, J. Y. & Meyer, I. M. R-CHIE: a web server and R package for visualizing RNA secondary structures. *Nucleic Acids Res* **40**, e95 (2012).
33. Cannone, J. *et al.* The Comparative RNA Web (CRW) Site: an online database of comparative sequence and structure information for ribosomal, intron, and other RNAs. *BMC Bioinformatics* **3**, 2 (2002).
34. Edgar, R. MUSCLE: multiple sequence alignment with high accuracy and high throughput. *Nucleic Acids Res* **32**, 1792–1797 (2004).
35. Griffiths-Jones, S. *et al.* Rfam: annotating non-coding RNAs in complete genomes. *Nucleic Acids Res* **33**, D121–D124 (2005).
36. Nussinov, R. & Jacobson, A. Fast algorithm for predicting the secondary structure of single-stranded RNA. *PNAS* **77**, 6309–6313 (1980).
37. Hofacker, I. *et al.* Fast Folding and Comparison of RNA Secondary Structures. *Monatshefte für Chemie (Chemical Monthly)* **125**, 167–188 (1994).
38. Lorenz, R. *et al.* ViennaRNA Package 2.0. *Algorithms for Molecular Biology* **6** (2011).

**Acknowledgements** This project was supported by grants to I.M.M. from the Natural Sciences and Engineering Research Council (NSERC) of Canada and from the Canada Foundation for Innovation (CFI). J.R.P. holds an Alexander Graham Bell Canada Graduate Scholarship from NSERC, with additional funding from the CIHR/MSFHR Bioinformatics Training Program at the University of British Columbia. CIHR are the Canadian Institutes of Health Research and MSFHR is the Michael Smith Foundation for Health Research in Canada.

**Author Contributions** Both authors were involved in every aspect of the research. J.R.P. programmed CoFOLD.

**Author Information** Correspondence and requests for material should be addressed to I.M.M. (irmtraud.meyer@cantab.net).

## Figures

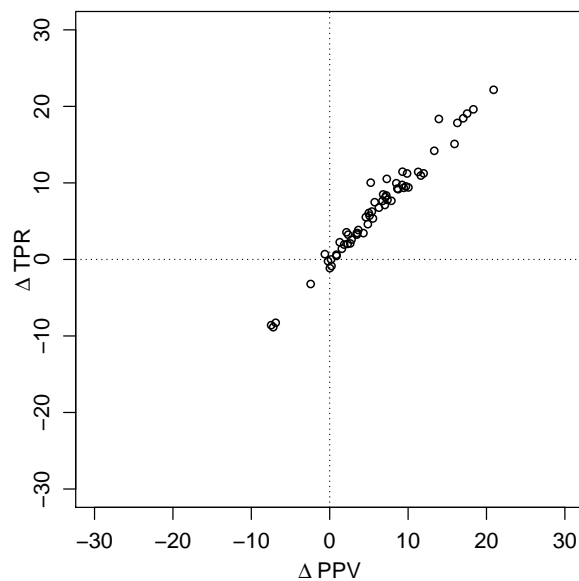


**Figure 1. Changes in prediction accuracy for the structures predicted by CoFold for individual sequences.** We report the prediction accuracy for base pairs of the long data set in terms of absolute changes of the true positive rate ( $TPR = 100 \cdot TP / (TP + FN)$ ) and the positive predictive value ( $PPV = 100 \cdot TP / (TP + FP)$ ) by comparing the prediction accuracy of the structures predicted by CoFold to those predicted by RNAfold. TP denotes the numbers of true positives, TN the true negatives, FP the false positives and FN the false negatives, see Supplementary Information Section 2 for detailed definitions.

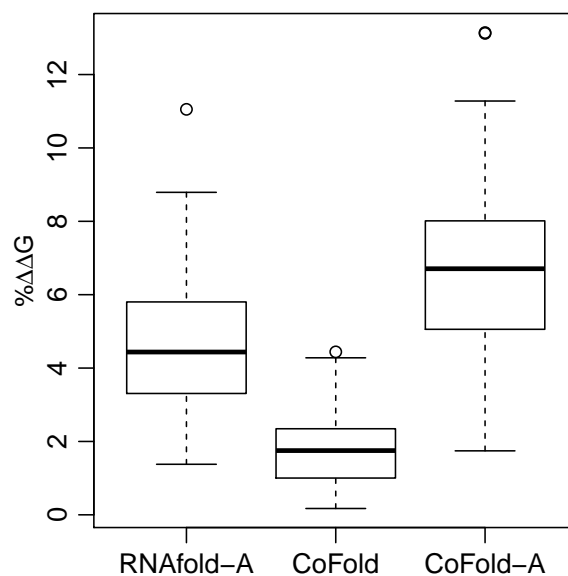


**Figure 2. Relative free energy differences of the predicted structures w.r.t. the MFE structures predicted by RNAFOLD.** Summary of three distributions for the long data set showing the relative free energy differences of the RNA structures predicted by RNAFOLD-A w.r.t. the MFE structures predicted by RNAFOLD for the same sequence (left), of the RNA structures predicted by CoFOLD w.r.t. the MFE structures predicted by RNAFOLD (middle) and of the RNA structures predicted by CoFOLD-A w.r.t the MFE structures predicted by RNAFOLD-A (right). The free energies of all structures are calculated using the Turner 1999 energy parameters. For each of the three distributions, the dark horizontal line indicates the average, the box indicates the 1st to the 3rd quartile, and the dotted lines indicate minimum and maximum values. Circles indicate outliers which are not included in the calculation of the average value.

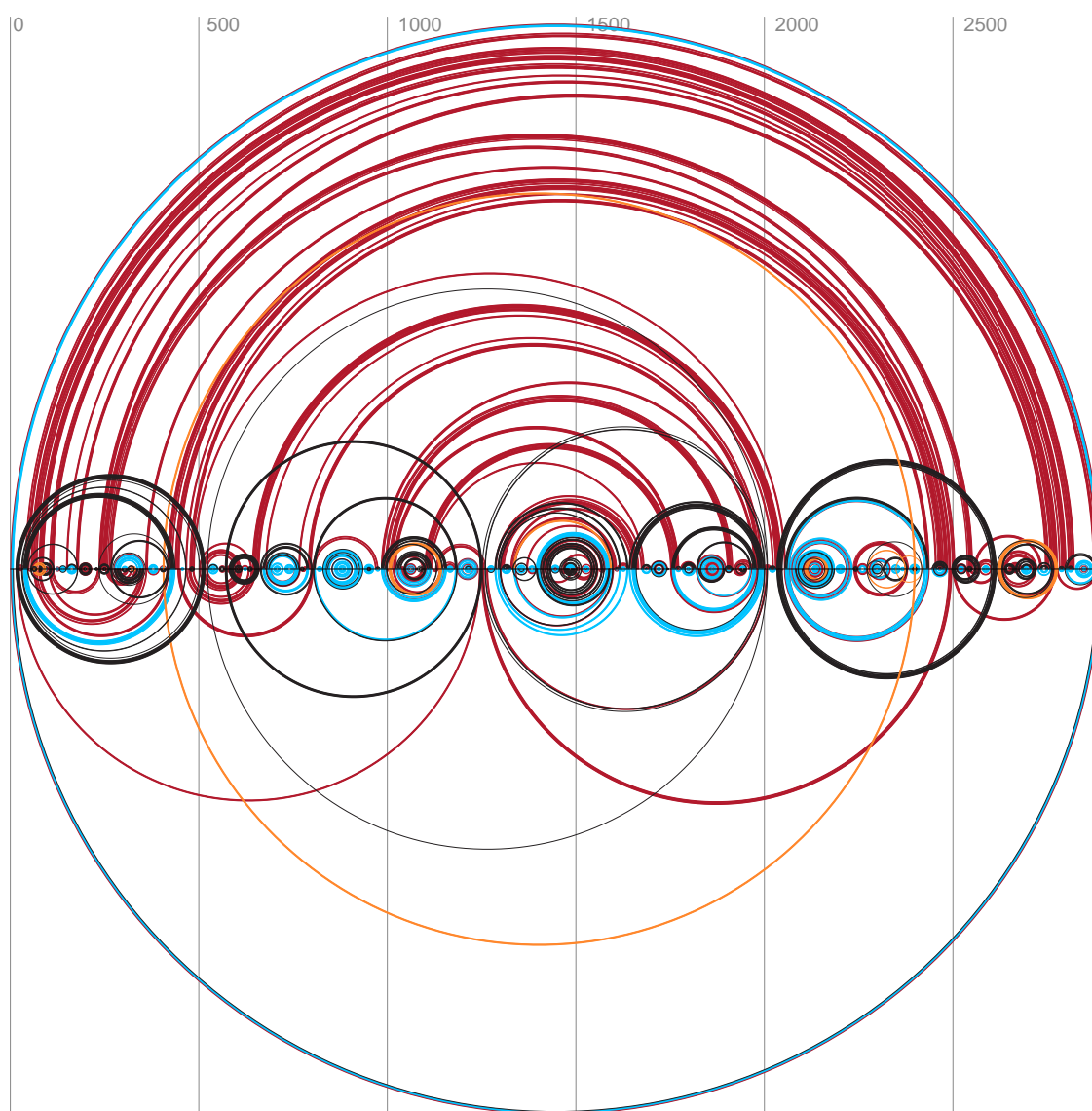


**Figure 3.** RNA  $\beta$ s predicted by CoFOLD-A and RNAfold for the 23S rRNA of the gamma-proteobacteria *Pseudomonas aeruginosa*. The horizontal line corresponds to the RNA sequence of 2893 nt length. The structure predicted by RNAfold is shown above the horizontal line, the one predicted by CoFOLD-A below. Each arc corresponds to a base-pair between the two corresponding positions along the sequence. Blue arcs correspond to correctly predicted base pairs (true positives), red arcs to incorrectly predicted base pairs (false positives) and black arcs to base pairs that are part of the reference structure, but missing from the prediction (false negatives). Orange arcs indicate base pairs of the reference structure that render it pseudo-knotted. Figure made with R-CHIE<sup>32</sup>.

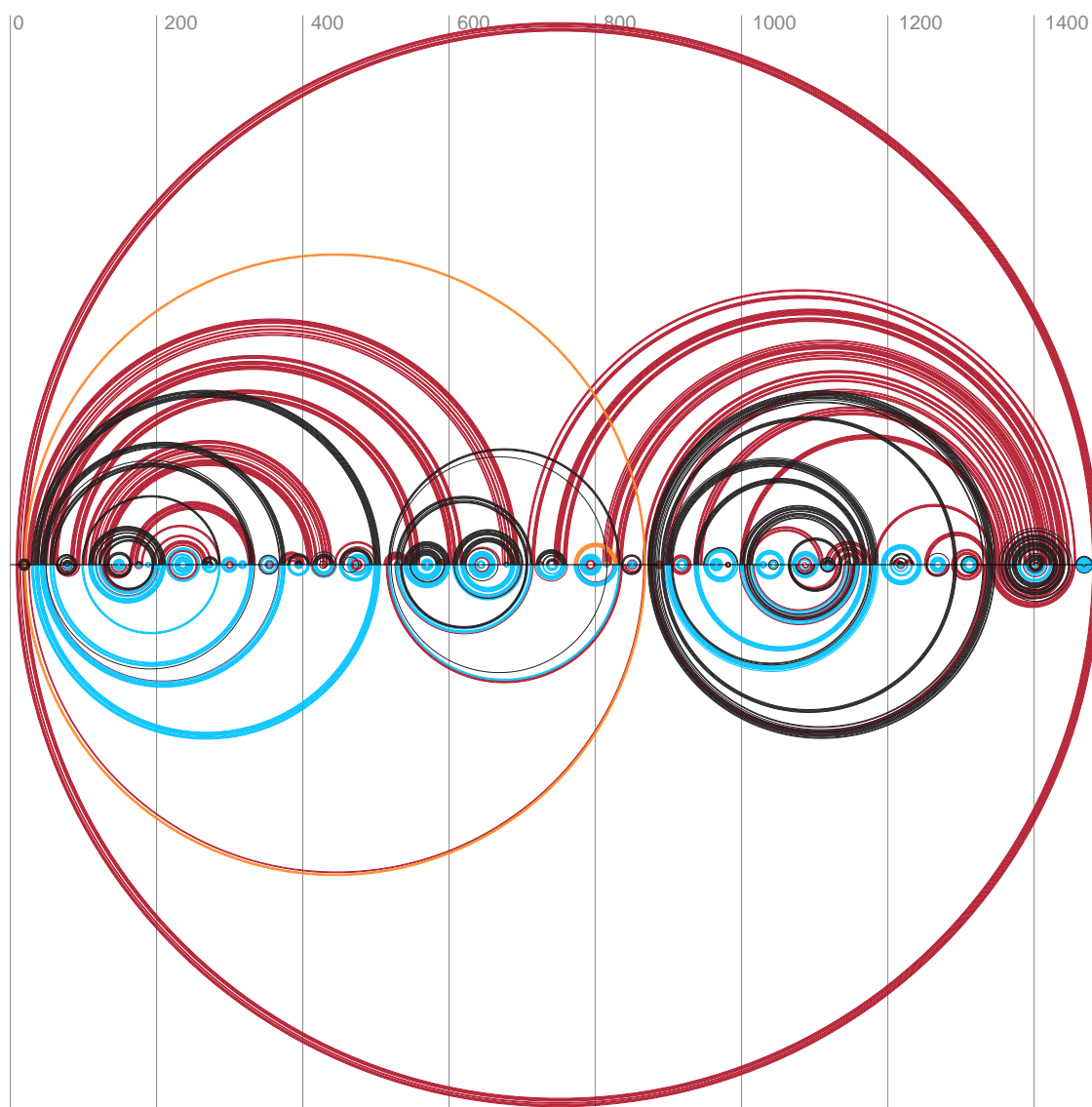


**Figure 4.** RNA  $\beta$ s predicted by COFOLD-A and RNAFOLD for the 16S rRNA of the freshwater algae *Cryptomonas sp.*. The horizontal line corresponds to the RNA sequence of 1493 nt length. The structure predicted by RNAFOLD is shown above the horizontal line, the one predicted by COFOLD-A below. Each arc corresponds to a base-pair between the two corresponding positions along the sequence. Blue arcs correspond to correctly predicted base pairs (true positives), red arcs to incorrectly predicted base pairs (false positives) and black arcs to base pairs that are part of the reference structure, but missing from the prediction (false negatives). Orange arcs indicate base pairs of the reference structure that render it pseudo-knotted. Figure made with R-CHIE<sup>32</sup>.

## Supplementary Information

### COFOLD: thermodynamic RNA structure prediction with a kinetic twist

Jeff R. Proctor and Irmtraud M. Meyer

Centre for High-Throughput Biology & Department of Computer Science and  
Department of Medical Genetics, University of British Columbia,

2125 East Mall, Vancouver, BC,  
Canada V6T 1Z4, irmtraud.meyer@cantab.net

July 15, 2012

#### Methods

**(1) Compilation of the long and combined data sets** The long data set consists of 16S and 23S ribosomal RNAs only. 16S and 23S multiple-sequence alignments for bacteria, eukaryotes, archaea and chloroplasts were retrieved from the Comparative RNA Web site (CRW)<sup>33</sup>. Because no consensus RNA structure is provided for each alignment, we projected the individual structures onto the alignment. The structure with the lowest mismatch score (defined in Equation (1)) was chosen as the consensus RNA structure for each alignment. For the calculation of the mismatch score, base pairs with a gap in one base position, and a non-gap in the other are considered one-sided gaps. Base pairs with gaps on both sides are considered two-sided gaps. Non-canonical pairs are those other than G-C, A-U, G-U. The length of the alignment  $A$  is denoted by  $|A|$ .

$$\text{mismatch} := \frac{\sum_{seq \in A} (2 \cdot (\# \text{ one-sided gaps}) + (\# \text{ two-sided gaps}) + (\# \text{ non-canonical pairs}))}{|A|} \quad (1)$$

Sequences with large indels, many ambiguous nucleotides, or a poor fit to the consensus RNA structure were removed from the alignment. Unpaired regions of the alignment were realigned using MUSCLE<sup>34</sup>. Individual sequences were extracted from each resulting alignment such that no pair of extracted sequences have a pairwise percent sequence identity greater than an alignment-specific threshold. The exact threshold varies to ensure no biological class or evolutionary clade is over-represented in the long data set (max 85%, Table 3). For each extracted sequence, the consensus alignment structure was projected onto the sequence by removing base pairs at gap positions, and removing any non-canonical base pairs. The resulting 61 sequences have a mean sequence length of 2397 nt and constitute the long data set (Table 2, Table 3 and Table 4).

The combined data set was constructed primarily for robustness of parameter training, and contains RFAM sequences from a wide variety of biological classes<sup>35</sup>. RFAM alignments were chosen according to the following criteria:

- mean sequence length greater than 115

- covariation (defined in Equation (2)) greater than 0.18
- minimum of 5 sequences
- mean percentage of canonical base pairs greater than 80%
- diverse biological classes and evolutionary clades

Sequences were extracted from the RFAM alignments using the same protocol as for the CRW alignments described above. Specifically, no pair of sequences extracted from the same alignment share a pairwise percent sequence identity above an alignment-specific threshold (max 85%, Table 3). Consensus RNA structures were projected onto individual sequences by removing base pairs at gap positions, and by removing any non-canonical base pairs. The mean sequence length of the resulting 187 RFAM sequences is 247 nt, and the combined dataset has an average sequence length of 778 nt (Table 2), see Table 3 for a description of biological class and sequence extraction details, and Table 4 for alignment quality metrics.

For a given multiple-sequence alignment, the covariation is defined as:

$$\text{covariation} := \frac{\sum_{a=1, b=1, a < b}^M \left( \sum_{S_{ij}} (\Pi_{ij}^{ab} H(a_i a_j, b_i b_j) - \Omega_{ij}^{ab} H(a_i a_j, b_i b_j)) \right) / (|S_{ij}|)}{\binom{M}{2}} \quad (2)$$

where

- $S_{ij}$  is the set of base pairs  $i$  and  $j$  in the consensus secondary structure.
- $M$  is the number of sequences in the alignment.
- $H(a_i a_j, b_i b_j)$  is the Hamming distance between the strings  $a_i a_j$  and  $b_i b_j$ .
- $\Pi_{ij}^{ab}$  is an indicator function such that if  $a_i$  and  $a_j$  can form a canonical base-pair, and  $b_i$  and  $b_j$  can also form a canonical base-pair,  $\Pi_{ij}^{ab} = 1$  (otherwise  $\Pi_{ij}^{ab} = 0$ ).
- $\Omega_{ij}^{ab}$  is an indicator function such that if  $a_i$  and  $a_j$  and/or  $b_i$  and  $b_j$  cannot form a canonical base-pair,  $\Omega_{ij}^{ab} = 1$  (otherwise  $\Omega_{ij}^{ab} = 0$ ).

**(2) Definition of performance metrics** Structure prediction accuracy is measured on a base pair level. True positives (TP) are correctly predicted base pairs. False positives (FP) are incorrectly predicted base pairs that are not part of the reference structure. True negatives (TN) are hypothetical base pairs that are not predicted, nor part of the reference structure. False negatives (FN) are reference base pairs missed by the prediction. Performance metrics for true positive rate (TPR), false positive rate (FPR), positive predictive value (PPV), and Matthew's correlation coefficient (MCC) are defined as follows:

$$TPR = 100 \cdot \frac{TP}{TP + FN} \quad (3)$$

$$\Delta TPR = TPR_{\text{CoFold}} - TPR_{\text{RNAfold}} \quad (4)$$

$$FPR = 100 \cdot \frac{FP}{FP + TN} \quad (5)$$

$$\Delta FPR = FPR_{\text{CoFold}} - FPR_{\text{RNAfold}} \quad (6)$$

$$PPV = 100 \cdot \frac{TP}{TP + FP} \quad (7)$$

$$\Delta PPV = PPV_{\text{CoFold}} - PPV_{\text{RNAfold}} \quad (8)$$

$$MCC = 100 \cdot \frac{TP \times TN - FP \times FN}{\sqrt{(TP + FP) \times (TP + FN) \times (TN + FP) \times (TN + FN)}} \quad (9)$$

### (3) Incorporating co-transcriptional folding into the prediction algorithm of CoFold

The Nussinov algorithm<sup>36</sup> was one of the first attempts at RNA  $\beta$  prediction. It is a dynamic programming method that efficiently calculates the  $\beta$  with the largest number of base pairs in  $O(L^3)$  time, where  $L$  denotes the length of the input sequence. The algorithm solves the problem recursively by determining the optimal structure for sub-sequences, and using these solutions to derive optimal structures for successively larger subsequences. The output structure is the optimal solution for the full sequence. This algorithm, however, has several shortcomings. First, base pairs vary in stability; for example, G-C pairs are energetically more favourable than A-U pairs. The Nussinov algorithm weights all pairs equally. Second, The stability of a base pair depends highly on its neighbouring base pairs due to so-called stacking interactions between adjacent pairs, and this contextual effect is ignored by the algorithm.

The Zuker-Stiegler algorithm<sup>3</sup> is an advancement of the Nussinov algorithm. Rather than predicting the structure with the greatest number of pairs, the Zuker-Stiegler algorithm predicts the most thermodynamically favourable (and pseudo-knot free) RNA structure according to a set of free energy parameters. This structure is also called the minimum-free-energy (MFE) structure. The algorithm assigns a sequence-specific free energy value to various structural building blocks, such as stacking interactions between pairs of adjacent base pairs, unpaired nucleotides, and hairpin loops. The algorithm utilises dynamic programming similarly to the Nussinov algorithm, but calculates two energy values for all subsequences  $S_{i,j}$  of a given input sequence  $S$ , where  $1 \leq i < j \leq L$ :

- $C_{i,j}$ : minimum free energy of subsequence  $S_{i,j}$  given nucleotides  $i$  and  $j$  form a base pair
- $FML_{i,j}$ : minimum free energy of subsequence  $S_{i,j}$

$$C_{i,j} = \min \begin{cases} \text{hairpin}_{i,j} & \text{open a helix with hairpin loop} \\ \min_{i < p < q < j} \{C_{p,q} + \text{Stack}_{(i,j),(p,q)}\} & \text{stack, bulge or internal loop} \\ \min_{k,l \in \{1,2\}} \{FML_{i+k,j-l} + \text{dangle}\} & \text{open a helix with nested substructure} \end{cases} \quad (10)$$

$$FML_{i,j} = \min \begin{cases} \min_{i < k < j} \{FML_{i,k} + FML_{k+1,j}\} & \text{branched structures} \\ \min_{k,l \in \{0,1\}} \{C_{i+k,j-l} + \text{dangle}\} & \text{close a helix} \\ FML_{i+1,j} + E_{\text{unpaired}} & \text{unpaired nucleotide} \\ FML_{i,j-1} + E_{\text{unpaired}} & \text{unpaired nucleotide} \end{cases} \quad (11)$$



$C_{i,j}$  and  $FML_{i,j}$  are calculated for each subsequence  $S_{i,j}$  as the minimum of a well-defined set of rules (Equation (10), Equation (11)). The minimum free energy can be retrieved from the value at  $FML_{1,L}$ , where  $L$  denotes the length of the input sequence. The corresponding MFE structure is retrieved by backtracking through the  $C_{i,j}$  and  $FML_{i,j}$  matrices.

The Zuker-Stiegler algorithm requires a large set of thermodynamic parameters. In 1999, the Turner group published one such model, which included a combination of experimentally measured energies and estimated values<sup>5</sup>. This parameter set (called Turner 1999 parameter set) is widely used by many state-of-the-art tools, including RNAFOLD<sup>37</sup> and MFOLD<sup>4</sup>. Andronescu *et al.* improved estimated values in the Turner 1999 parameter set by applying sophisticated machine learning techniques to training 363 free parameter values<sup>6</sup>. These parameters were adjusted using a training set of 3439 reference structures and 946 thermodynamic measurements by optical melting resulting in the Andronescu 2007 parameter set. They observed an average performance increase of 7% on a test set of 1660 sequences containing several biological classes, including tRNA, RNase P, rRNA and SRP RNA.

The Zuker-Stiegler algorithm traditionally considers only the change in free energy for a given RNA  $\beta$  conformation in thermodynamic equilibrium, but does not consider the process of RNA structure formation, *i.e.* how the RNA sequence arrives at the MFE structure. Rather, the Zuker-Stiegler algorithm implicitly assumes that the input RNA sequence (1) is already fully synthesised, (2) in thermodynamic equilibrium and (3) will always be able to reach the RNA structure that minimises the overall free energy of the molecule. We know from a range of experiments, however, that RNA molecules start to fold while they emerge during transcription, that they are not necessarily in thermodynamic equilibrium during structure formation *in vivo* and that they may get trapped on their kinetic folding pathway. That RNA molecules overall proceed towards the MFE structure over time is only an approximation of the complex reality *in vivo*. As the molecule emerges from the polymerase, however, local structures immediately begin to form. Formation of long-range base pairs may require disruption of these local structures, and their folding rate may be prohibitively slow due to high energy barriers. That is, the molecule may never reach the minimum free energy structure due to kinetic considerations. The structure formation *in vivo* may get further complicated due *trans* interactions between the RNA sequence and other molecules in the living cell which we ignore for now.

We propose a new method for RNA  $\beta$  prediction, CoFOLD, that takes into account some effects of co-transcriptional folding. The key effect that we aim to model is that during co-transcriptional folding *in vivo*, it does matter to a given sequence position whether a potential pairing partner is available for base-pairing or not. To capture this, we model the distance along the sequence between base pairing sequence positions. CoFOLD is a modification to the Zuker-Stiegler algorithm<sup>3</sup>, and it was implemented using the RNAFOLD source code from the VIENNARNA package<sup>37,38</sup>.

CoFOLD calculates energies in the same fashion as in RNAFOLD, but all energy contributions associated with a base pair are modified by a scaling function according to the number of nucleotides between the pair (*i.e.* the distance  $d$ ). This scaling function  $\gamma(d)$  models the exponential decay in reachability as function of the nucleotide distance  $d$  between the two potential pairing partners and depends on two parameters  $\alpha$  and  $\tau$  (Equation (12), Figure 6). Both parameters have a straightforward interpretation. The value of  $\alpha$  specifies the range of the scaling function (*e.g.* when  $\alpha$  is 0.2, the affected free energies will range from 80% to 100% of their

original values). The value of  $\tau$  determines the rate of the exponential decay, where low values of  $\tau$  result in a steep decay function.

$$\gamma(d) := \alpha \cdot (e^{-\frac{d}{\tau}} - 1) + 1 \quad (12)$$

The scaling function  $\gamma(d)$  is only used in conjunction with energy values in the  $C_{i,j}$  calculation because these correspond to predicted base pairs. The function is not applied to the energy of subsequences in order to avoid multiple applications to the same value. The function is applied both to elements with positive energy, such as loops and bulges, as well as to those with negative energy, such as stacking interactions. This is necessary to preserve the relative magnitude of the contributions from structural components, see Equation (13) and Figure 7 for modified  $C'_{i,j}$ . The  $FML_{i,j}$  calculation remains the same as in RNAFOLD.

$$C'_{i,j} = \min \begin{cases} \gamma(d_{i,j}) \cdot \text{hairpin}_{i,j} & \text{open a helix with hairpin loop} \\ \min_{i < p < q < j} \{C_{p,q} + \gamma(d_{i,j}) \cdot \text{Stack}_{(i,j),(p,q)}\} & \text{stack, bulge or internal loop} \\ \min_{k,l \in 1,2} \{FML_{i+k,j-l} + \gamma(d_{i,j}) \cdot \text{dangle}\} & \text{open a helix with nested substructure} \end{cases} \quad (13)$$

The output of CoFOLD is an RNA  $\beta$  which promotes base pairs according to the above scaling function. The predicted RNA  $\beta$  therefore captures both thermodynamic contributions as well as effects due to co-transcriptional structure formation. Like RNAFOLD, CoFOLD allows the user to select a thermodynamic parameter set and the running time of CoFOLD also scales with  $O(L^3)$ , where  $L$  denotes the length of the input sequence. For performance evaluation, we use both the Turner 1999 (CoFOLD) and the Andronescu 2007 (CoFOLD-A) parameter sets introduced above.

**(4) Parameter training** CoFOLD has two free parameters:  $\alpha$  and  $\tau$ . Due to the small number of parameters, they were trained using a simple brute force scheme. CoFOLD was run on all sequences of the combined data set and performance metrics were calculated for each  $(\alpha, \tau)$  combination in set  $P$  (defined in Equation (14)). The Turner 1999 thermodynamic parameter set<sup>5</sup> was used for  $(\alpha, \tau)$  parameter training.

$$P := \{0.05, 0.10, \dots, 0.90, 0.95\} \times \{40, 80, \dots, 1160, 1200\} \quad (14)$$

$$\overline{MCC}_{\alpha,\tau}^S := \frac{\sum_{s \in S} MCC_{\alpha,\tau}^s}{|S|} \quad (15)$$

where  $(\alpha, \tau) \in P$  and  $S$  is the sequence set

$$\overline{\Delta MCC}_{\alpha,\tau}^S := \overline{MCC}_{\alpha,\tau}^S - \overline{MCC}_{\text{RNAfold}} \quad (16)$$

Performance metrics were found to be highly correlated in  $\alpha$  and  $\tau$  (Figure 8 (right), Figure 9). To demonstrate this, linear regression was performed on the  $\overline{\Delta MCC}$  matrix (Figure 8 (left)). We first compiled a set of triples  $Q = \{(\alpha, \tau, \overline{\Delta MCC}_{\alpha,\tau})\}$ , for which  $\overline{\Delta MCC}_{\alpha,\tau}$

is in the 97<sup>th</sup> quantile of the performance matrix. Weighted linear regression was performed with  $\alpha$  and  $\tau$  as dimensions, and  $\overline{\Delta MCC}$  as the weight. The regression line fits the data with an  $R^2$  value of 98.4%, indicating that variability in  $\tau$  highly accounts for the variability in  $\alpha$ . Regression line (solid) and its 95% confidence region (dotted) are plotted in Figure 8 (left).

Twenty trials of five-fold cross validation were performed to determine robustness of parameter training. In each trial, the combined data set  $D$  is randomly divided into five partitions  $D_i$ . For each partition, the optimal parameter combination is determined for the remaining sequences (Equation (17)). The cross validation results are plotted in Figure 8 (right), where the integer in each cell indicates the number of trials where that parameter combination was optimal. The optimal parameter values highly cluster around the linear regression line show in Figure 8 (left).

$$(\alpha_{opt}, \tau_{opt}) := (\alpha, \tau) \text{ s.t. } \overline{\Delta MCC}_{\alpha, \tau}^T = \max(\overline{\Delta MCC}^T) \quad (17)$$

where  $T := D \setminus D_i$

The default parameter combination for CoFOLD is  $\alpha = 0.5, \tau = 640$ . This parameter set maximises  $\overline{MCC}$  for the combined dataset. The default parameter combination is marked with an "X" in Figure 8 (left) which shows that it lies directly on the linear regression line.

**(5) Calculation of free energy differences** We define  $\Delta\Delta G$  as the difference between the free energy ( $\Delta G$ ) of a given prediction and the corresponding RNAfold prediction. We calculate these values for RNAfold-A, CoFOLD, and CoFOLD-A. Because the Andronescu 2007 parameters use modified the free energy values, we use RNAeval from the VIENNA RNA package<sup>37,38</sup> to calculate the free energy of each predicted structure on an equal footing. Unlike RNAfold which predicts a minimum free energy structure from a sequence, RNAeval calculated the free energy for an input RNA structure according to the provided thermodynamic parameters. For consistency, we use the parameters Turner 1999 thermodynamic model<sup>5</sup> for all  $\Delta\Delta G$  calculation. For a prediction program  $X$  which corresponds to RNAfold-A CoFOLD or CoFOLD-A, we define  $\Delta\Delta G_X$  and  $\% \Delta\Delta G_X$  as follows.

$$\Delta\Delta G_X = \Delta G_X - \Delta G_{\text{RNAfold}} \quad (18)$$

$$\% \Delta\Delta G_X = 100 \cdot \frac{(\Delta G_X - \Delta G_{\text{RNAfold}})}{|\Delta G_{\text{RNAfold}}|} \quad (19)$$

## Tables

clade	long data set	combined data set	
	> 1000 nt	all	≤ 1000 nt
Bacteria	15	69	(54)
Eukaryotes	15	112	(97)
Virus	0	20	(20)
Archea	17	33	(16)
Chloroplast	14	14	(0)
sum	61	248	(187)
sequence length (nt)			
average	2397	776	(247)
minimum	1245	110	(110)
maximum	3578	3578	(628)

**Table 2. Evolutionary composition and length statistics for the long and the combined data set.** Numbers in brackets specify the respective numbers for the short sequences in the combined data set.

biological class	A.len (nt)	clade	N.seq	N.ext	max ppid (%)	source	ID
16S rRNA (archaea)	1545	A	40	8	85	CRW	16S archaea
23S rRNA (archaea)	3153	A	40	9	85	CRW	23S archaea
16S rRNA (bacteria)	1661	B	144	7	70	CRW	16S bacteria
23S rRNA (bacteria)	3046	B	40	8	85	CRW	23S bacteria
16S rRNA (chloroplast)	1558	C	40	5	85	CRW	16S chloroplast
23S rRNA (chloroplast)	3722	C	40	9	80	CRW	23S chloroplast
16S rRNA (eukaryote)	1867	E	40	7	85	CRW	16S eukaryote
23S rRNA (eukaryote)	4105	E	40	8	85	CRW	23S eukaryote
snRNA	184	E	87	14	80	RFAM	RF00003
U2 spliceosomal RNA	270	E	181	10	50	RFAM	RF00004
Nuclear RNase P	622	E	77	11	45	RFAM	RF00009
snoRNA	236	E	14	9	85	RFAM	RF01256
snoRNA	394	E	4	1	85	RFAM	RF01267
snoRNA	373	E	18	9	85	RFAM	RF01296
U4 spliceosomal RNA	273	E	160	11	50	RFAM	RF00015
U5 spliceosomal RNA	178	E	153	9	45	RFAM	RF00020
ciliate telomerase RNA comp.	270	E	19	11	80	RFAM	RF00025
RNase MRP	903	E	40	12	50	RFAM	RF00030
RNase P	511	B	88	8	60	RFAM	RF00011
CsrB RNA	391	B	11	7	85	RFAM	RF00018
lysine riboswitch	232	B	37	14	65	RFAM	RF00168
Mg riboswitch - Ykok leader	216	B	85	14	65	RFAM	RF00380
Ornate extremophilic RNA	676	B	7	6	85	RFAM	RF01071
Pestivirus IRES	286	V	23	5	85	RFAM	RF00209
Tombusvirus 5' UTR	180	V	7	5	85	RFAM	RF00171
Aphthovirus IRES	471	V	87	4	85	RFAM	RF00210
Cripavirus IRES	208	V	6	6	80	RFAM	RF00458
tRNA-like structures	137	V	5	5	80	RFAM	RF01084
Archaeal RNase P	533	A	25	16	80	RFAM	RF00373

**Table 3. RNA families of the long and the combined data set.** All sequences of the long data set derive from alignments of the CRW data base (top), whereas the short sequences from the combined data set all derive from alignments of the RFAM data base (bottom). For each original alignment from either data base, *i.e.* each row in this table, we specify the alignment length in nucleotides (A.len), the evolutionary origin of its sequences (clade, A - Archea, B - Bacteria, C - Chloroplast, V - Virus, E - Eukaryotes), the number of sequences (N.seq), data base (source) and identifier in that data base (ID). We also specify, for each original alignment, how many sequences we extracted (N.ext) and what their maximum pairwise percent identify is in terms of primary sequence conservation (max. ppid). IRES stands for internal ribosomal entry site.

alignment (ID)	A.len (nt)	av. seq. length (nt)	av. ppid (%)	gaps (%)	n (%)	bpairs	canonical bpairs (%)	covar.
16S archaea	1545	1477	81.8	4.4	$5 \cdot 10^{-7}$	458	95.2	0.343
23S archaea	3153	2945	74.9	6.6	$6 \cdot 10^{-7}$	852	95.0	0.408
16S bacteria	1661	1520	76.7	8.5	$2 \cdot 10^{-2}$	453	93.4	0.352
23S bacteria	3046	2904	79.2	4.6	$6 \cdot 10^{-7}$	868	94.3	0.358
16S chloroplast	1558	1490	90.2	4.4	$5 \cdot 10^{-7}$	440	93.9	0.113
23S chloroplast	3722	2941	74.8	21.0	0	869	90.1	0.253
16S eukaryote	1867	1708	73.3	8.5	$1 \cdot 10^{-7}$	370	84.3	0.162
23S eukaryote	4105	3476	78.7	15.3	$1 \cdot 10^{-7}$	998	88.1	0.084
RF00003	184	162	63.1	11.8	0	40	93.2	0.493
RF00004	270	193	58.4	28.4	$1 \cdot 10^{-2}$	45	92.8	0.496
RF00009	622	315	40.7	49.3	$8 \cdot 10^{-5}$	62	89.3	0.397
RF01256	236	208	60.6	11.9	0	54	92.7	0.457
RF01267	394	384	72.5	2.6	0	128	94.3	0.295
RF01296	373	325	63.7	13.0	0	57	91.4	0.339
RF00015	273	147	52.2	46.2	$5 \cdot 10^{-5}$	31	91.5	0.604
RF00020	178	117	51.7	34.1	$4 \cdot 10^{-5}$	30	94.0	0.694
RF00025	270	186	42.5	31.1	0	39	86.4	0.395
RF00030	903	303	34.7	66.5	0	74	88.3	0.470
RF00011	511	373	63.0	27.1	0	105	95.1	0.500
RF00018	391	350	62.4	10.5	0	49	96.8	0.368
RF00168	232	183	46.1	21.2	0	53	90.3	0.580
RF00380	216	170	59.6	21.4	0	47	94.5	0.471
RF01071	676	609	59.9	9.9	0	159	90.2	0.378
RF00209	286	275	89.2	3.9	0	75	98.8	0.191
RF00171	180	159	67.3	11.4	0	34	97.9	0.403
RF00210	471	461	85.4	2.1	0	122	98.3	0.181
RF00458	208	201	55.4	3.5	0	60	95.0	0.757
RF01084	137	128	51.0	6.9	0	43	97.2	0.795
RF00373	533	311	49.4	41.7	0	87	90.0	0.537

**Table 4. Alignment quality and phylogenetic support for the reference RNA  $\beta$ s.**

For each original alignment, *i.e.* each row in this table, we specify the alignment length in nucleotides (A.len), the average length of each non-gapped sequence in that alignment (av. seq. length), the average pairwise percent identity between pairs of sequences in the alignment in terms of primary sequence conservation (av. ppid), the average fraction of gaps per sequence in the alignment (gaps), the average fraction of ambiguous (not A,C,G,T,U,-) nucleotide symbols per sequence in the alignment (n), the number of base pairs in the reference RNA  $\beta$  for that alignment (bpairs), the average fraction of sequences in the alignment that have a consensus base-pair per conserved base-pair of the reference  $\beta$  (canonical bpairs) and the covariation (covar.) as defined in RFAM<sup>35</sup> which measures how well the base pairs of the reference RNA  $\beta$  are supported by co-variation (high means good).

long data set				
	TPR (%)	FPR (%)	PPV (%)	MCC (%)
RNAFOLD	46.30	0.0176	39.74	42.81
RNAFOLD-A	52.02	0.0160	44.76	48.17
CoFOLD	52.83	0.0159	45.79	49.10
CoFOLD-A	57.80	0.0145	50.06	53.70
combined data set				
	TPR (%)	FPR (%)	PPV (%)	MCC (%)
RNAFOLD	57.87	0.1132	45.27	50.86
RNAFOLD-A	58.98	0.1152	46.16	51.83
CoFOLD	60.38	0.1097	47.56	53.26
CoFOLD-A	61.51	0.1112	48.42	54.22
short sequences only				
	TPR (%)	FPR (%)	PPV (%)	MCC (%)
RNAFOLD	61.64	0.1444	47.08	53.48
RNAFOLD-A	61.25	0.1475	46.61	53.02
CoFOLD	62.84	0.1403	48.14	54.62
CoFOLD-A	62.72	0.1428	47.88	54.39

**Table 5. CoFOLD predictive power for base pairs for all data sets.** The performance accuracy of CoFOLD and CoFOLD-A compared to RNAFOLD and RNAFOLD-A for the test set as measured in terms of true positive rate ( $TPR = 100 \cdot TP / (TP + FN)$ ), false positive rate ( $FPR = 100 \cdot FP / (FP + TN)$ ), positive predictive value ( $PPV = 100 \cdot TP / (TP + FP)$ ) and Matthew’s correlation coefficient ( $MCC = 100 \cdot (TP \cdot TN - FP \cdot FN) / \sqrt{(TP + FP) \cdot (TP + FN) \cdot (TN + FP) \cdot (TN + FN)}$ ), where TP denotes the numbers of true positives, TN the true negatives, FP the false positives and FN the false negatives.

Summary of % $\Delta\Delta G$ distributions									
	long data set			combined data set					
	> 1000 nt			all			$\leq 1000$ nt		
	av. $\pm$ stdev	min	max	av. $\pm$ stdev	min	max	av. $\pm$ stdev	min	max
RNAFOLD-A	4.7 $\pm$ 1.9	1.4	11.1	5.0 $\pm$ 3.5	-2.3	15.4	5.1 $\pm$ 3.9	-2.3	15.4
CoFOLD	1.8 $\pm$ 1.0	0.2	4.4	0.5 $\pm$ 1.2	-5.0	4.4	0.1 $\pm$ 0.9	-5.0	3.8
CoFOLD-A	6.8 $\pm$ 2.4	1.7	13.1	5.9 $\pm$ 3.8	-2.3	18.2	5.6 $\pm$ 4.1	-2.3	18.2

**Table 6. Summary of relative free energy difference distributions of predicted structures w.r.t. the MFE structured predicted by RNAFOLD for the same input sequences, for all data sets.**

Linear fit to $\Delta$ MCC versus % $\Delta\Delta$ G distributions			
long data set			
> 1000 nt			
	intercept $\pm$ stdev	slope $\pm$ stdev	R <sup>2</sup> (%)
RNAFOLD-A	7.0 $\pm$ 2.4	-0.34 $\pm$ 0.48	0.85
CoFOLD	3.5 $\pm$ 1.6	1.52 $\pm$ 0.78	6.06
CoFOLD-A	9.2 $\pm$ 3.1	0.25 $\pm$ 0.43	0.56
combined data set			
	intercept $\pm$ stdev	slope $\pm$ stdev	R <sup>2</sup> (%)
RNAFOLD-A	1.0 $\pm$ 1.4	0.0008 $\pm$ 0.23	5.6 $\cdot$ 10 <sup>-06</sup>
CoFOLD	2.1 $\pm$ 0.6	0.59 $\pm$ 0.47	0.64
CoFOLD-A	2.1 $\pm$ 1.6	0.21 $\pm$ 0.23	0.34
short sequences only			
$\leq$ 1000 nt			
	intercept $\pm$ stdev	slope $\pm$ stdev	R <sup>2</sup> (%)
RNAFOLD-A	-0.8 $\pm$ 1.6	0.06 $\pm$ 0.25	0.03
CoFOLD	1.3 $\pm$ 0.7	-2.21 $\pm$ 0.75	4.44
CoFOLD-A	0.7 $\pm$ 1.7	0.03 $\pm$ 0.25	0.01

**Table 7. Details of the linear fits to the  $\Delta$  MCC versus %  $\Delta\Delta$ G distributions.**



## Figures

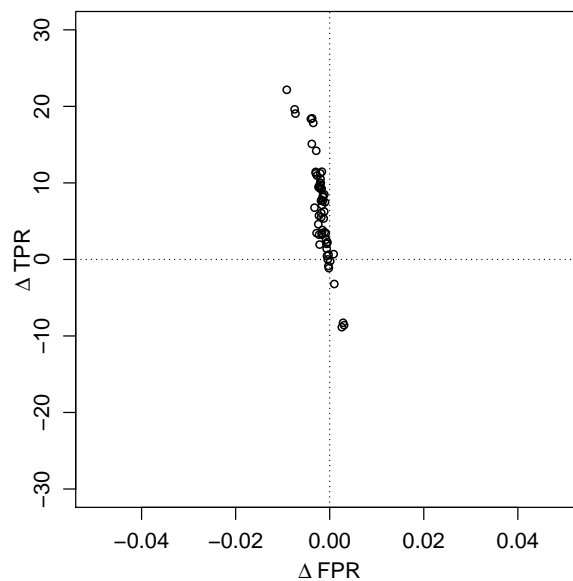


**Figure 5. Changes in prediction accuracy for the structures predicted by CoFold for all sequences of the long data set.** We report the prediction accuracy for base pairs in terms of relative changes in true positive rate ( $TPR = 100 \cdot TP / (TP + FN)$ ) and false positive rate ( $FPR = 100 \cdot FP / (FP + TN)$ ) by comparing the prediction accuracy of the structures predicted by CoFold to those predicted by RNAfold. TP denotes the numbers of true positives, TN the true negatives, FP the false positives and FN the false negatives.

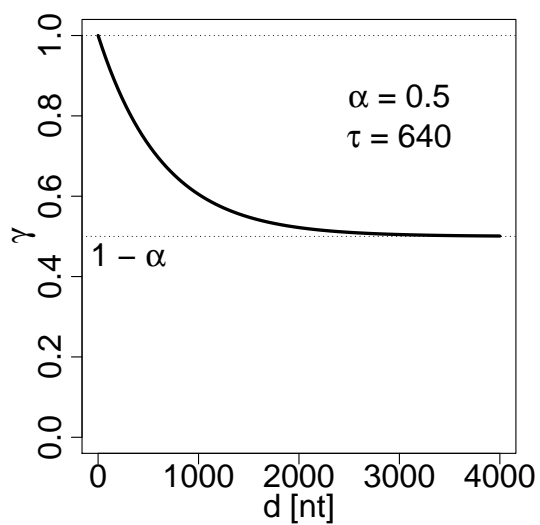


Figure 6. Scaling function  $\gamma$  of CoFOLD.

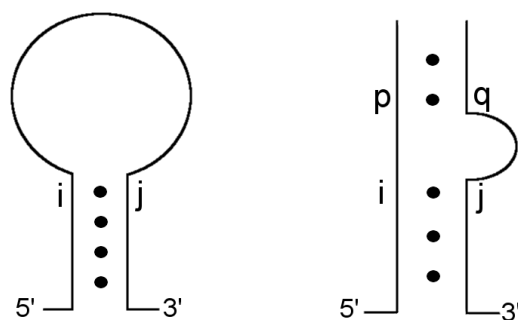
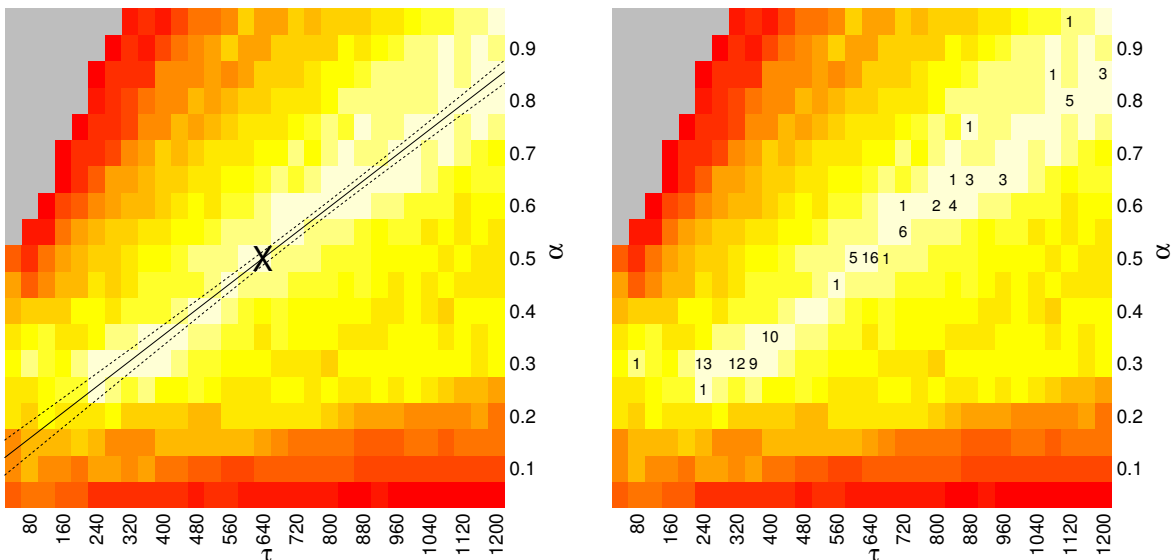
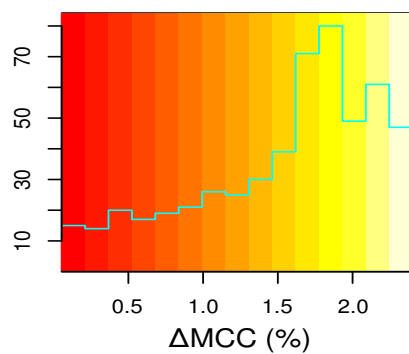


Figure 7. Details of the sequence coordinates affected by the scaling function of CoFOLD in Equation (13).



**Figure 8. Training of parameters in CoFOLD: linear fit and robustness.** Left figure, heatmap showing the average MCC differences w.r.t. RNAFOLD as function of the  $\tau$  (x-axis) and  $\alpha$  (y-axis) parameters values. The average MCC differences are indicated via the colours from high (bright yellow) to low (dark red), see Figure 9 for details. The solid line corresponds to the linear regression line ( $\alpha = a \cdot \tau + b$  with a slope of  $a = 6.1 \cdot 10^{-4} \pm 2 \cdot 10^{-5}$  and an intercept of  $b = 0.105 \pm 0.016$ ). The two dotted lines delineate the 95% confidence region. The asterisk shows parameter pair with highest average MCC ( $\alpha = 0.50$  and  $\tau = 640$ ) which is the parameter combination used in CoFOLD and CoFOLD-A. Right figure, same heatmap as in left figure, but this time showing the count of trials in 20 trials of five-fold cross-validation where that the corresponding pair of parameter values has the highest average MCC for the set of training sequences.



**Figure 9. Colour coding for the heatmaps for parameter training of CoFold.** Histogram of the average MCC differences of CoFold w.r.t. RNAFold, ranging from light yellow for the largest improvement of performance accuracy to dark red for a small performance improvement. A grey colour in Figure 8 corresponds to an improvement accuracy that is smaller than the range covered in this histogram.

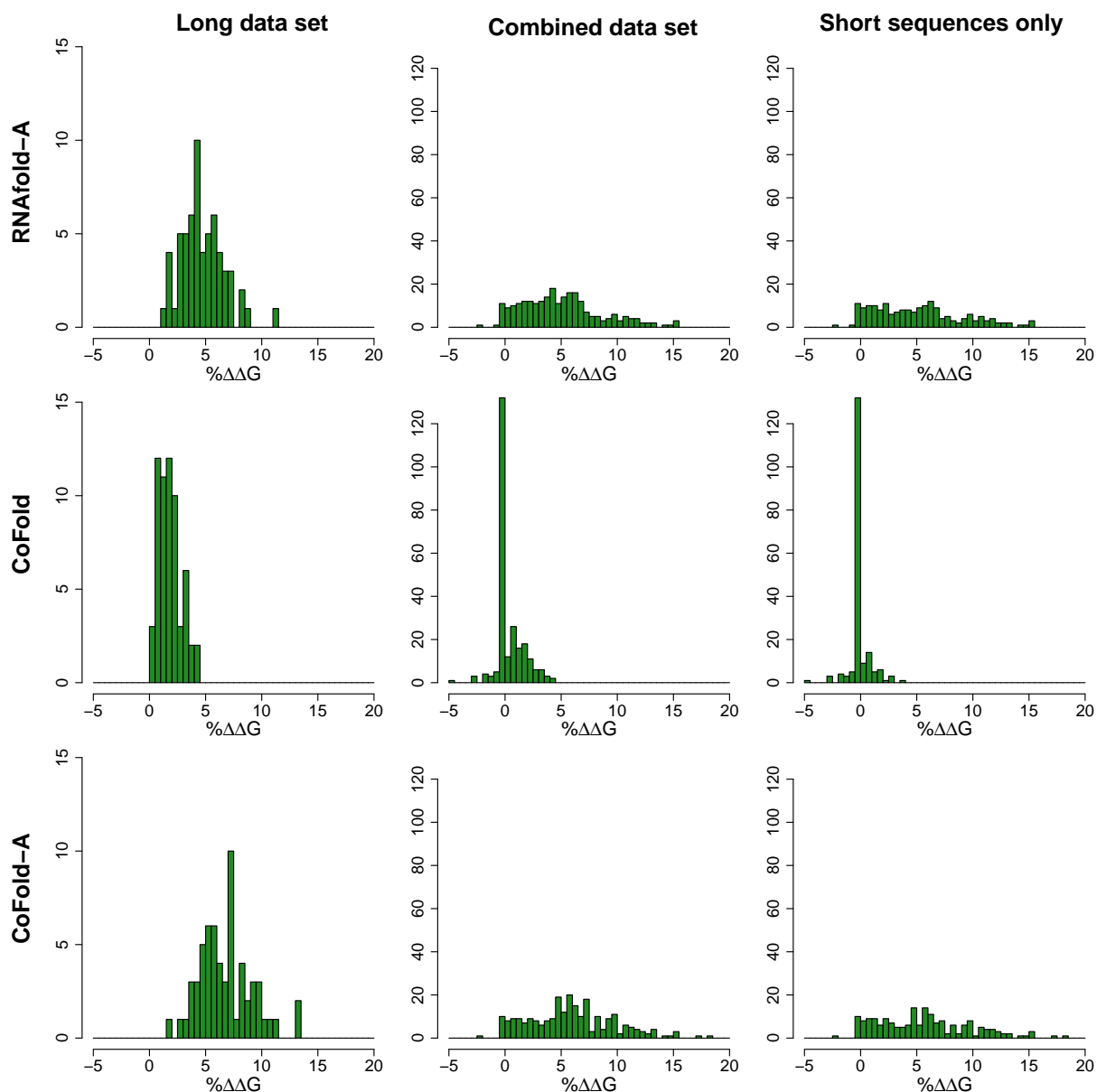


**Figure 10. Relative free energy difference distributions of the predicted structures w.r.t. the MFE structures predicted by RNAFOLD for the same input sequences, for all data sets.** Results for the long data set (left column), the combined data set (middle column) and the short sequences of the combined data set (right column). For each data set, three histograms show the relative free energy differences of the RNA structures predicted by RNAFOLD-A w.r.t. the MFE structures predicted by RNAFOLD for the same sequence (top row), of the RNA structures predicted by CoFOLD w.r.t. the MFE structures predicted by RNAFOLD (middle row) and of the RNA structures predicted by CoFOLD-A w.r.t. the MFE structures predicted by RNAFOLD-A (bottom row). The free energies of all structures are calculated using the Turner 1999 energy parameters.

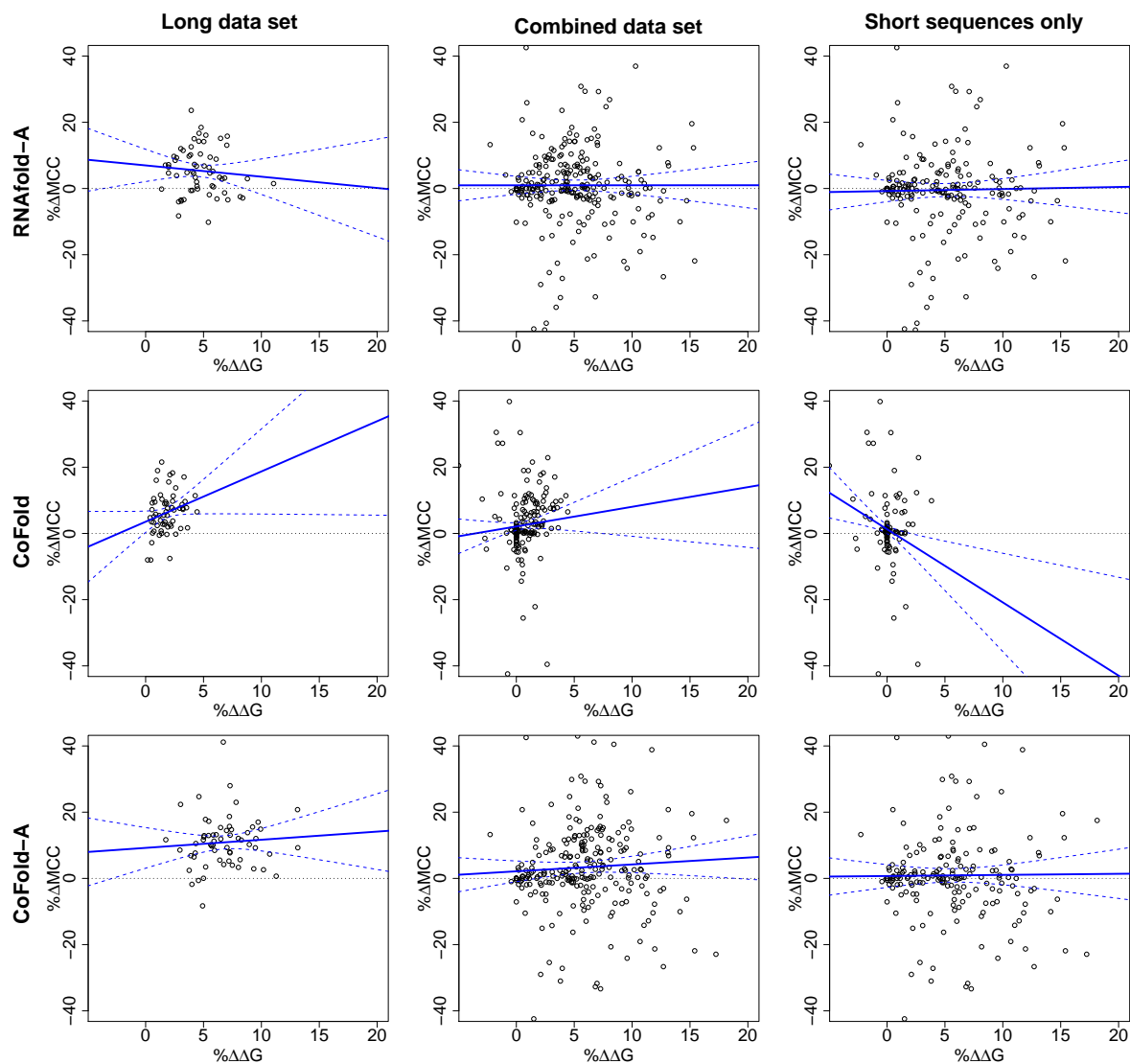


**Figure 11. Differences in prediction accuracy versus relative free energy changes of the predicted structures w.r.t. the MFE structures predicted by RNAFOLD for the same input sequences, for all data sets.** Results for the long data set (left column), the combined data set (middle column) and the short sequences of the combined data set (right column). For each data set, three figures show the change in performance accuracy in terms of MCC versus the relative change of free energy for the structures predicted by RNAFOLD-A (top row) w.r.t. the RNA structures predicted by RNAFOLD for the same sequence, for the structures predicted by COFOLD (middle row) w.r.t. the RNA structures predicted by RNAFOLD for the same sequence and for the structures predicted by COFOLD-A (bottom row) w.r.t. the RNA structures predicted by RNAFOLD for the same sequence. The free energies of all structures are calculated using the Turner 1999 energy parameters.